Intensified upwelling: normalized sea surface temperature trends expose climate change in coastal areas

Miguel Ángel Gutierrez-Guerra[1,2], María Dolores Pérez-Hernández[1], Pedro Vélez-Belchí[2]

[1] Unidad Océano y Clima, Instituto de Oceanografía y Cambio Global, IOCAG, Universidad de Las Palmas de Gran Canaria, ULPGC, Unidad Asociada ULPGC-CSIC, Canary Islands, Spain

[2] Centro Oceanográfico de Canarias, Instituto Español de Oceanografía, Santa Cruz de Tenerife, Canary Islands, Spain

Corresponding author: Miguel A. Gutierrez-Guerra, miguel.gutierrez104@alu.ulpgc.es

Abstract.

The Eastern Boundary Upwelling Systems (EBUS) provide valuable natural resources due to their high primary production. However, there is significant uncertainty in how climate change may affect the mechanisms that sustain these ecosystems in the future. Therefore, assessing the effects of climate change on the EBUS under the current global warming scenario is crucial for efficient ecosystem management. In 1990, Andrew Bakun suggested an increase in the upwelling intensity due to the rise of the ocean-land pressure gradient. Since there is a significant link between thermal gradients and offshore Ekman transport, we use sea level pressure and deseasonalized sea surface temperature (SST) data from remote sensing to elucidate this hypothesis and validate it using in-situ observations. SST is an indicator of coastal upwelling, and our long-term analysis of monthly and deseasonalized SST records shows that the seasonal and synoptic processes have minimal influence on the SST-upwelling intensity relationship. Upwelling within the same EBUS is not usually evenly distributed along coastlines, leading to upwelling in specific areas, upwelling centers. We compare the SST trends in the main upwelling centers of the four EBUS with those in open ocean waters through a new index, α_{UI}, designed to characterize upwelling changes in the EBUS. An adimensional number allows us to normalize the trends independently of the upwelling system and compare all of them. Furthermore, we have complemented the SST index with sea level pressure gradient data. This new index (supported by SLP gradient trends) indicates intensification in all the EBUS, revealing a coherent pattern within EBUS in the same ocean (i.e., Canarian and Benguela or Californian and Humboldt Upwelling Systems).

1. Introduction

The world's major coastal upwelling areas exist along the eastern margins of the Pacific and the Atlantic Oceans. These extended coastal upwelling systems are known as Eastern Boundary Upwelling Systems (EBUS) and sustain the most important fisheries in the world (Pauly and Christensen, 1995). The rise of cool, nutrient-rich waters supports the high primary production needed to maintain these complex ecosystems (Ekman, 1905). Their economic and ecological relevance explains the association of the EBUS with the world's major Large Marine Ecosystems (LME) (Fig 1). LME are a globalized approach to a management framework that defines and ranks marine regions based on their gross primary production (Sherman and Hempel, 2008), and four of the largest LME are embedded in the EBUS worldwide (Kämpf and Chapman, 2016).

Bakun, (1990) hypothesized that the sea-land temperature gradient will increase under climate change and therefore, it should increase the upwelling intensity. The hypothesized increase in the temperature gradient arises from an increased atmospheric pressure gradient between the low-pressure cell that develops over the heated land mass and the high-pressure cell existing over the colder ocean. Therefore, as the land warms faster than the ocean, it enhances the low-pressure cells. Thus, the increase in the pressure gradient drives more intense upwelling favorable winds, intensifying the cold imprint in the Sea Surface Temperature (SST) near the shore. However, previous studies that have tested Bakun's hypothesis with in-situ data have found contradictory long-term trends (Barton et al., 2013; Belkin, 2009; McGregor et al., 2007; Rykaczewski et al., 2015; Sambe et al., 2016).
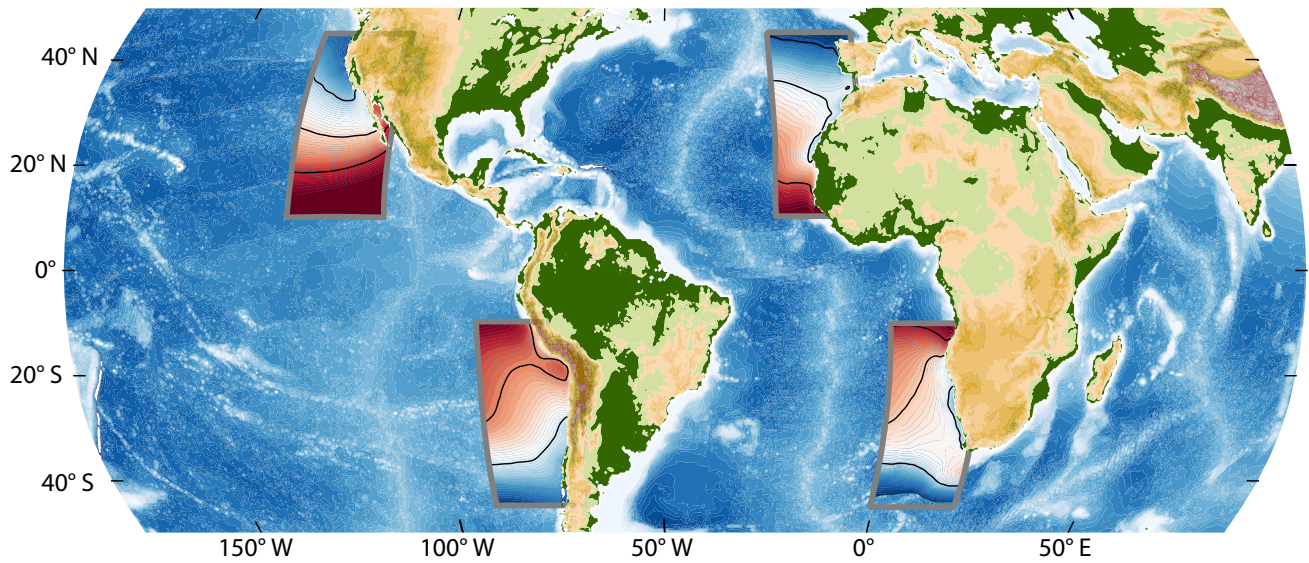
Fig 1: Location of the EBUS (colored areas) in the world, associated with eastern boundary currents. For each region, the enclosed area includes the mean SST from 1982-2022.

47 Sydeman et al., (2014) performed a meta-analysis of 18 trends obtained from independent studies of wind
48 stress, both from observational and model data. Observational data were more likely to report an increase
49 in wind stress in the four EBUS than model data (excluding Benguela, where no observations were
50 considered). However, the model data were less consistent between EBUS, showing agreement with
51 observations only in the case of the California system (both supporting intensification) and for the Iberian
52 system (with a consistent weakening of the wind stress). García-Reyes et al., (2015) also remarked that
53 in climate change models, the upwelling-related cooling trends were difficult to reproduce due to the
54 small spatial scale of the coastal upwelling process. Such a controversy between the model, and different
55 observations reflects the complexity of EBUS dynamics.

56 Upwelling within the same EBUS is not usually evenly distributed along coastlines because of irregular
57 coastlines and seafloors, leading to more pronounced upwelling in specific areas known as 'upwelling
58 centers' (Kämpf and Chapman, 2016). These centers are characterized by strong frontal areas and
59 upwelling jets that create eddies. In these areas, the sea surface temperature drops due to the upwelling of
60 cold subsurface water. Therefore, the relationship between sea surface temperature (SST) and the
61 upwelling intensity is more robust in these upwelling centers. Even in cases where a generalized increase
62 in favorable upwelling winds occurs, the appearance of cold SST cores, associated with increased

63 upwelling intensity, remains predominantly confined to these specific areas. Therefore, to study the long-
64 term changes in the upwelling, a good approach is to focus on these representative upwelling areas within
65 the EBUS since they show a higher signal-to-noise ratio between the SST and Ekman transport.

66 The main motivation of this study is to assess the impacts of climate change on the four EBUS. This is
67 pursued by using satellite-derived SST trends as a proxy for changes and a new index that normalizes the
68 upwelling trend of the coastal upwelling with the oceanic background trends. Specifically, we have
69 chosen points representative of each dynamical regime at each EBUS: offshore oceanic waters (OC1),
70 non-upwelling (DW1) areas nearshore, and upwelling centers (UP1 and UP2). These points were chosen
71 based on the consistency of the year-round upwelling centers deduced from the mean SST field and the
72 relevance of the area as spawning and nursery emplacements for the pelagic fisheries associated with
73 upwelling centers. Then, we compare the SST trends in the main upwelling centers of the four EBUS
74 with those in open ocean waters through a new index, α_{UI}, designed to characterize upwelling changes in
75 the EBUS, following Bakun's (1990) hypothesis. The manuscript is organized as follows: sections 2 and
76 3 describe the dataset and the analysis carried out in the study. Section 4 describes the relevant results,
77 and the results are discussed and contrasted with other studies, and finally, Section 5 summarizes and
78 presents the conclusions.

79 **2. Data**

80 We based our study on the SST blended analyses for sea surface temperature of the National Ocean and
81 Atmosphere Administration (NOAA) (Reynolds et al., 2007), which combines SST satellite retrievals
82 with in-situ measures from ships and buoys. This dataset has a spatial resolution of 0.25º and covers
83 nearly 40 years (from 1982 to 2021). Following Barton et al. (2013), the 40-years used in this study allow
84 us to estimate significant trends. Their analysis involved a comprehensive examination of both wind stress
85 and SST. They segmented these datasets into various subsets of different lengths. Within this analysis,
86 the trends derived from wind datasets are not significantly different from zero for all considered subset
87 periods.

88 In contrast, SST trends demonstrated statistical significance with a dataset of 40-years length. In addition,
89 we incorporated reliable in-situ data in the North Pacific and the North Atlantic oceans for validation.

These records were obtained from the National Buoy Data Center (NDBC) and the CalCOFI (California Cooperative Fisheries Investigations) program for the Pacific. For the Atlantic, the data were gathered from Puertos del Estado and the RaProCan (Radial Profunda de Canarias) observational program of the Spanish Institute of Oceanography in the Canary Islands (Tel et al., 2016). The in-situ data, limited to the northern hemisphere, is used to validate the satellite observations. Given the significantly larger amount of sampling density existing in the Pacific Ocean compared to the Atlantic Ocean, a lower error is expected in the reanalysis for the Pacific Ocean. We have also used the EN4 (ENhanced ocean data assimilation and climate Prediction) dataset from the Met Office Hadley Centre (Good et al., 2013), a collection of global observations from diverse sources interpolated into a monthly product and a spatial resolution of 1º. Due to the limited sampling in the cruise data, we cannot align it with the monthly resolution of the EN4 product. To maintain statistical rigor, we choose not to employ the cruise data for the validation of EN4.

Additionally, two sea level pressure (SLP) datasets are used: the NCEP and ERA5 reanalysis data. The ERA5, from the European Centre for Medium-Range Weather Forecasts, offers a high resolution of ~0.25 degrees and uses advanced data assimilation methods, covering the period from 1950 to present. While the NCEP/NCAR Reanalysis, from the National Centers for Environmental Prediction and the National Center for Atmospheric Research, offers a resolution of 2.5 degrees and uses covering the period from 1948 to present.

3. Method

3.1. Selection of Representative Dynamical Regimes in EBUS.

We have selected areas representative of the different dynamical regimes for further analysis, to avoid mixing observations in dynamically different areas. Areas UP1 and UP2 are round-year upwelling centers. The DW1 are areas of convergence where the upwelling does not dominate on an annual average, and these areas are characterized by higher SST averages than those in the upwelling centers. The OC1 is representative of open ocean (>100km offshore) areas with trends driven by Global Warming. Given

115 the distinctive and unique features that characterised each EBUS, as commented in Section 1, we based
116 the selection of the representative locations on the literature and the SST mean field (Fig. 2):

117 **Californian Upwelling System (CaIUS)**

118 In the Californian system, the strongest wind stress takes place in spring in the southern portion of the
119 CalUS. In summer the strongest winds occur offshore of northern California around 38° N. This wind
120 stress pattern diminishes as we move away from this latitude in both directions (Bakun and Nelson, 1991).
121 Among the four regions depicted by Kämpf and Chapman (2016), the strongest upwelling occurs in two
122 well-known upwelling centers that we have selected for the analysis in this study: Cape Mendocino
123 (Abbott and Zion, 1987) and Point Conception (Dugdale and Wilkerson, 1989), south of it, the wind's
124 seasonal variability is different.

125 **Canarian Upwelling System (CanUS)**

126 Following Kämpf and Chapman (2016), the CanUS is divided into two distinct upwelling areas, which
127 experience limited continuity of flows between them. This division arises due to the coastline interruption
128 in the Strait of Gibraltar that leads to two upwelling areas: the Iberian Upwelling System and the Canarian
129 Upwelling System. Given the lack of permanent upwelling centers in the Iberian Upwelling System, we
130 have focused on the Canarian Upwelling System. Following Cropper et al. (2014), we selected the two
131 upwelling centers (UP1 and UP2) on the cold SST cores (see Fig 2b) within the permanent upwelling
132 area.

133 **Humboldt Upwelling System (HuUS)**

134 The HuUS is characterized by prominently strong upwelling zones along the Peruvian-Chilean coastline,
135 due to the topographical influence of headlands, as described by Figueroa & Moffat, (2000) and Mesias
136 et al., (2003). Notable regional upwelling centers encompass the continental shelf near Pisco (13.7° S),
137 Antofagasta (21-25º S), and the Mejillones Peninsula (23° S), as well as extending further south to
138 Coquimbo Bay (30° S), Valparaíso (33° S), and the Bay of Concepción (37° S). Moreover, in the
139 Mejillones Peninsula (23° S), both observational (e.g., Marín, 2003) and modeling studies (Escribano et

140 al., 2004) have revealed that the dynamics of coastal ecosystems in this area heavily rely on the generation
141 of upwelling filaments. Additionally, the continental shelf near Pisco (13.7° S) emerges as an
142 exceptionally productive and distinctive upwelling center. Hence, the two upwelling centers selected are
143 the Mejillones Peninsula and Pisco.

Benguela Upwelling System (BeUS)

145 As Kämpf and Chapman (2016) described, within the Benguela Upwelling System, numerous upwelling
146 centers extend along the shelf area of the Benguela Current region. These centers include Cape Frio (18.5°
147 S), Walvis Bay (22.95° S), Lüderitz (26.45° S), Namaqualand (28.55° S), Cape Columbine (32.85° S),
148 and Cape Town (33.95° S). Lüderitz stands out as a particularly noteworthy upwelling center within this
149 system (Andrews and Hutchings, 1980; Lutjeharms and Meeuwis, 1987; Peard, 2007). As Hutchings et
150 al. (2009) defined, Lüderitz represents an intensive perennial upwelling center characterized by intense
151 winds, high turbulence, and robust offshore transport. Another significant area of interest lies in Cape
152 Columbine, primarily due to its biological importance (Andrews and Hutchings, 1980; Bang and
153 Andrews, 1974; Andrews and Cram, 1969). Given these distinctive features, we have selected Lüderitz
154 and Cape Columbine as the upwelling centers for our analysis.

3.2. Trends Analysis

156 With a minimum data length (>30 years), a climate series can usually be described as a combination of
157 multiple variabilities at different time scales. Since we are interested in the trend of the record, we
158 removed the high-frequency variability (<1 yr) by averaging the daily NOAA SST analyses data (1982-
159 2021) into monthly means and removing the seasonal cycle. The seasonal cycle is a recursive signal
160 throughout the entire record, and therefore, it does not influence the trend but induces noise in the target
161 scale. The monthly climatology was subtracted from the record to remove the seasonal cycle. After this
162 pre-analysis, we calculated the trend with the ordinary least square method. We evaluated the strength of
163 these correlations using the Pearson Correlation Coefficient (PCC). The following qualitative
164 classification will be used throughout the manuscript: Perfect (1), very high (>0.9), high (>0.7), and
165 moderate (>0.5). Additionally, we employed the simple Mann-Kendall (MK) test to evaluate the statistical

166 robustness (Kendall, 1975; Mann, 1945). The MK tests verify whether an n-length series holds a
167 monotonic increase or decrease trend. In addition, we need to consider the instrumental error since,
168 historically, a warm coastal bias is found in satellite records compared to in-situ records (Smale and
169 Wernberg, 2009). This bias was assessed in the northern hemisphere by validating the data using in-situ
170 observations. Additionally, to assess the drivers of change in upwelling intensity, we calculated the sea
171 level pressure (SLP) gradients for each EBUS. The gradients were calculated between the cores of the
172 high- and low-pressure systems (exact positions provided in supplementary material, Fig S1). To
173 corroborate the Rykaczewski hypothesis, we used the spatial standard deviation. A displacement of the
174 pressure systems would increase the standard deviation of the trends around their cores.

175 **3.3. Angular Index of Upwelling Intensification (α_{UI})**

176 To test Bakun's hypothesis, a new index, named the Angular Index of Upwelling Intensification (α_{UI}), is
177 proposed. This new index uses the angle between the trend of the most robust upwelling cell at each
178 EBUS and the trend at the corresponding open ocean area. If the upwelling intensifies, as Bakun proposed,
179 the trends in the open ocean and the cell are expected to differ significantly, resulting in a higher angle
180 between the trends. To calculate α_{UI}, two vectors (in the time-temperature space) may be constructed from
181 the upwelling ($\overline{Up}$) and oceanic ($\overline{Oc}$) trends. The rotation sense (clockwise or anticlockwise) is used to
182 calculate the relative orientation of ($\overline{Up}$) over ($\overline{Oc}$), needing to consider an additional unit vector ($\bar{n}$)
183 normal to $\overline{Up}$ and $\overline{Oc}$

184 The mathematical formulation of α_{UI} is

$$\alpha_{UI} = arctan^* \left(\frac{((\overline{Up} \; x \; \overline{Oc}) \cdot \bar{n})}{\overline{Up} \cdot \overline{Oc}} \right) = arctan \left(\frac{|\overline{Up}||\overline{Oc}| \; sin(\alpha_{UI})}{|\overline{Up}||\overline{Oc}| \; cos(\alpha_{UI})} |\bar{n}|cos(\beta) \right)$$

186 [*] We used the four-quadrants arc tangent in this analysis since it allows to determine the sign of the
187 angle based on the signs of the arguments.

188 Following the right-hand rule, if the cross product of ($\overline{Up}$) and ($\overline{Oc}$) is anticlockwise (that is, if the open
189 ocean trend ($\overline{Oc}$) is greater than the upwelling trend ($\overline{Up}$), the resulting vector of the cross product has the
190 same orientation as $\bar{n}$. This implies that the dot product ($\overline{Up}$) x ($\overline{Oc}$)·$\bar{n}$ is positive since the angle (β)
191 between $\bar{n}$ and ($\overline{Up}$ x $\overline{Oc}$) is 0º. In case the upwelling trend is greater than the open ocean trend, $\overline{Up}$ x $\overline{Oc}$

192 results negative since β is now 180º. Note that this methodology is susceptible to the order of the vectors,

193 as $\overline{Up}$ x $\overline{Oc}$=-$\overline{Oc}$ x $\overline{Up}$. Since we are interested in the relative position of the upwelling trend concerning

194 the oceanic waters, the order used is $\overline{Up}$ x $\overline{Oc}$. It is important to note that the angle derived from

195 trigonometric functions are not influence by units associated with the original vectors. Therefore, this

196 new index is independent of temperature and time units.

197 We also conducted a probabilistic assessment of uncertainties for α_{UI}, taking into account the uncertainties

198 associated with upwelling and open ocean SST series. We performed an error estimation using the Monte

199 Carlo method: individual data points were separately and randomly sampled 10,000 times within their

200 respective $\overline{(Up)}$- and $\overline{(Oc)}$- uncertainty ranges. These new sampled series were then used to calculate

201 α_{UI}. The standard deviation of the 10,000 simulations represents the uncertainty of α_{UI}.

202 **3.4. Satellite Validation**

203 Taking advantage of the in-situ observations available in the study areas defined in Fig 2, we performed

204 a validation through linear regression between in-situ and the deseasonalized satellite data. Records with

205 no systematic error correspond to a linear regression slope with a value of 1 (perfect). Since the Pacific

206 Ocean is better sampled than the Atlantic, better reanalysis performance and higher correlation are

207 expected in the Pacific Ocean.

208 **4. Results**

209 **4.1. Satellite Validation**

210 We first carried out a regional validation, in the northern hemisphere, with in-situ observations (Fig 2a

211 and 2b) to test the consistency of the NOAA SST analyses between oceans. A linear fit between in-situ

212 and satellite data gives insights into the reliability of the SST data in both oceans. As described in Section

213 2, the in-situ dataset was divided into two categories: mooring and cruise data. Because each record has

214 a different spatial and temporal resolution, categories are not comparable.

a) SST climatological mean of CalUS
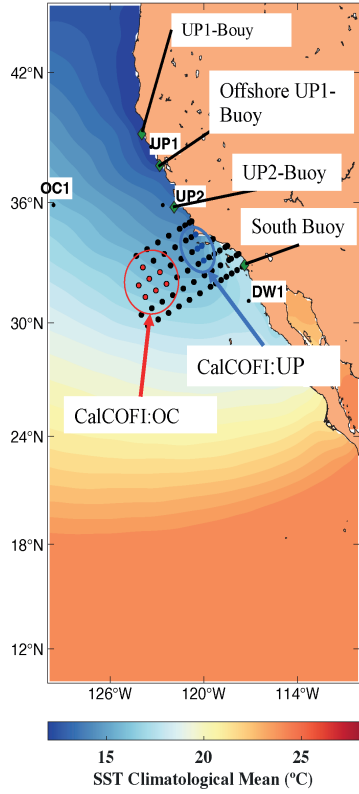
b) SST climatological mean of CanUS
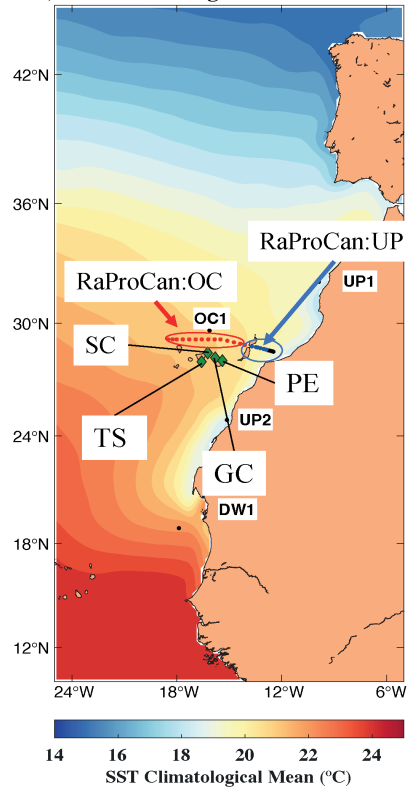
c) SST climatological mean of HuUS
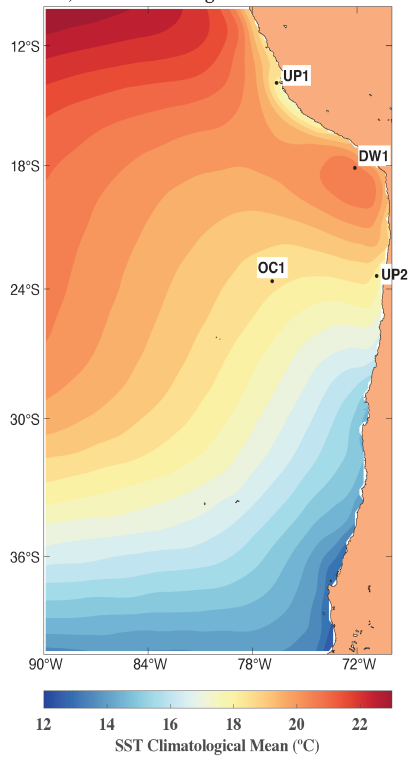
d) SST climatological mean of BeUS
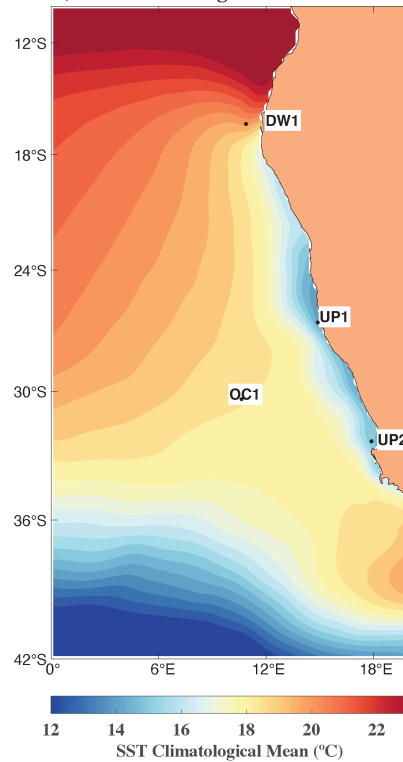
Fig 2: Average SST maps for each of the Upwelling Systems: CalUS (a), CanUS (b), HuUS (c), and BeUS (d). Overlaid are the locations of the moorings (green diamond) and cruise data (black dots) used for the satellite validation with their corresponding names. The cruise stations were divided into upwelling and open ocean areas marked with blue and red circles, respectively. The representative points of UP, DW, and OC in each basin are shown as black dots.

215 In the Pacific Ocean, the moorings selected were those as close as possible to the areas UP1, UP2, DW1,
216 and OC1 described in section 3.1 and 3.4. We found the highest correlations inside the upwelling center
217 of this region, where the UP1-Buoy and UP2-Buoy presented a linear regression fit of 0.99, supported by
218 a very high correlation strength (0.94 and 0.92, respectively, Table 1). In the area where the upwelling
219 meets the oceanographic background, the correlation of the offshore UP1-Buoy with the NOAA SST data
220 decays slightly, presenting a linear slope of 0.84 and a correlation strength of 0.86. For the South-Buoy,
221 close to DW1, the lineal fit and correlation (0.97 and 0.92) are closer to the values inside of the upwelling
222 cell than of the offshore UP1-Buoy (Table 1). The results obtained for the offshore UP1-Buoy exemplify
223 the effect of using an average large area surrounding the upwelling centers instead of a point, as the
224 average introduces noise by adding points where upwelling might not be taking place, reducing the
225 correlation in the transitional zone.

226 The cruise observations in the Pacific Ocean (CalCOFI) were divided into two different areas, open ocean
227 (CalCOFI: OC) and upwelling (CalCOFI: UP), and we avoid data at transitional areas, as seen in Fig 2a.
228 The results of the linear fit between the cruise and the reanalysis data are similar to those obtained with
229 the mooring data (Table 1 and supplementary material Fig S2). The average within the upwelling cell,
230 CalCOFI: UP, has a very high linear regression value (0.91), while for the offshore stations, CalCOFI:
231 OC, the regression is 0.81. Nevertheless, the strength of the correlation is sensitive to the amount of data
232 available from the cruise data in the ocean versus the upwelling areas. Additionally, due to the time
233 resolution of the cruise, the correlation strength is moderate (0.68) for the CalCOFI: OC and high (0.71)
234 for the CalCOFI: UP.

235 We also compared the EN4 dataset (Table 1, two last columns) against the NOAA SST analysis. As
236 described in section 2, due to the coarse temporal resolution of the cruise data, it was not possible to
237 compare with the EN4 monthly. Overall, the EN4 has lower correlation and regression values than the
238 NOAA SST analyses. The correlation has the same pattern in both datasets (NOAA and EN4): moderate

239 in the northern locations (0.60 and 0.63) and high in the southern locations (both with 0.76), although the
240 data length of the EN4, unlike the cruise records, is the same as the mooring.

| | NOAA | | EN4 | |
In-situ Data	Linear Slope	Correlation	Linear Slope	Correlation
UP1-Buoy (46014).	0.99	0.92	0.70	0.60
Offshore UP1-Buoy (46028).	0.84	0.86	0.72	0.63
UP2-Buoy (46225).	0.99	0.94	0.78	0.76
South-Buoy (46026).	0.97	0.92	0.77	0.76
CalCOFI: OC	0.81	0.71	-	-
CalCOFI: UP	0.91	0.68	-	-

241 **Table 1. Values of the linear regression and Pearson's correlation strength between the in-situ data (listed in the**
242 **first column, with the designation within the manuscript and, in brackets, the official NDBC station ID). The in-**
243 **situ data are compared with the NOAA SST reanalysis (second and third columns) and the EN4 product (last two**
244 **columns) validation for the Pacific Ocean. The last two rows are for the CALCOFI cruise data of the Pacific**
245 **Ocean.**

246 In the Atlantic Ocean, the number of in-situ measurements available is more limited than in the Pacific
247 Ocean. Therefore, the long-term records are shorter than in the Pacific Ocean and are only available in
248 the surroundings of the Canary Islands. The results reflect these limitations since none of the linear
249 regressions or correlation coefficients ever exceeds 0.9, unlike the results for the Pacific Ocean (Table 1).
250 As in the Pacific Ocean, the mooring data shows a better linear regression and higher correlation
251 coefficient than the cruise data (Table 2 and supplementary material, Fig S3). The correlation coefficients
252 for the buoys of Santa Cruz, Gran Canaria, and Tenerife Sur are high, with values of 0.89 (0.84), 0.84
253 (0.87), and 0.83 (0.88), respectively. The result of Las Palmas East-Buoy is comparable to the linear slope
254 for the cruise data, 0.71. However, the Las Palmas East-Buoy has a higher correlation coefficient (0.89),
255 which agrees with the other moorings.

256 For the cruise data, we follow the same approach as in the Pacific Ocean, dividing the data into open
257 ocean areas (RaProCan: OC) and upwelling centers (RaProCan: UP). As occurred for the results in the
258 Pacific, the regression is better for the upwelling cell with values of 0.73 and a correlation strength of
259 0.71. For the open ocean areas (RaProCan: OC), the linear slope is slightly lower (0.63) but has a higher
260 correlation strength coefficient (0.77).

261 The EN4 dataset was also used in these areas and showed linear regressions and correlation coefficients
262 similar to the cruise data, as shown in Table 1. In Table 2, the linear regressions of EN4 are close to the
263 results of the moorings, even though EN4 performs similarly compared to Table 1. Thus, EN4 seems a
264 better alternative in the Atlantic Ocean than in the Pacific Ocean, but only due to the lower performance
265 of the NOAA SST analyses in the Atlantic Ocean. However, the correlation strength of the EN4 showed
266 lower values than NOAA SST analyses, with three out of five locations under 0.70. Hence, using the
267 NOAA SST analyses for long-term analysis in both oceans is a better approach.

	NOAA		EN4	
In-situ Data	Linear slope	Correlation	Linear Slope	Correlation
Las Palmas East Buoy.	0.71	0.89	0.80	0.71
Santa Cruz Buoy.	0.89	0.84	0.71	0.66
Gran Canaria Buoy.	0.84	0.87	0.76	0.54
Tenerife South Buoy.	0.83	0.88	0.77	0.53
RaProCan: OC	0.63	0.77	-	-
RaProCan: UP	0.73	0.71	-	-

268 **Table 2. Values of the linear fit and correlation strength between in-situ data (listed in the first column) and both**
269 **the NOAA SST analyses (second and third columns) and the EN4 product (last two columns) for the Atlantic**
270 **Ocean. The last two rows are for the RaProCan cruise data of the Atlantic Ocean.**

271 **4.2. Trend patterns on the EBUS**

272 We begin by identifying the overall pattern of the long-term trends in each EBUS, which we show in Fig
273 3. A general pattern of cooling (negative) trends within the upwelling centers and warming (positive)
274 trends offshore is found in most of the regions. An exception is found in the HuUS, where there is also a
275 cooling trend offshore. This cooling mode, however, is not as pronounced as the trends onshore driven
276 by the upwelling process. On top of these general patterns, each region presents unique features that will
277 be described in the following paragraphs.

278 The mean trend for the CalUS (Fig 3a) is 0.10 (SD= 0.06) ºC/decade. The minimum values, -0.17
279 ºC/decade, are located near Cape Mendocino, around 43-39ºN, and 32ºN corresponding to the permanent
280 upwelling centers. On the other hand, maximum values (excluding the shallower Gulf of California),

281 reaching up to 0.20 ºC/decade, are located south, at 30ºN, where the winds are non-favorable for year-
282 round upwelling, and there is convergence (Kämpf & Chapman, 2016). At around 22 ºN, there is an
283 offshore negative trend area with mean values of -0.02 ºC/decade. However, the MK test revealed that
284 these trends in the offshore area are not significant. The non-significant extensive regions in the MK test
285 support the idea that the trends in the CalUS coastal upwelling are only statistically distinguishable from
286 zero within the upwelling centers.

287 In the CanUS (Fig 3b), the mean trend in the region is warmer than in CalUS, with a value of 0.20 (SD=
288 0.04) °C/decade. The minimum values (-0.20 ºC/decade) are confined to two upwelling centers in the
289 permanent annual upwelling zones, located north of Cape Ghir and south of Cape Bojador. The maximum
290 warming trend is 0.60°C/decade, located west of Cape Timiris in the Mauritania-Senegalese convergence
291 zone. Because of the low spatial variability of the trend in the CanUS, the mean offshore value is the same
292 as the average value of the entire CanUS.

293 For the HuUS (Fig 3c), the mean value of the region is 0.007 (SD= 0.09) ºC/decade. a cooling signal
294 stands out as the general pattern in the tropic, with a mean value of -0.15 ºC/decade. Despite this cooling
295 of the overall trend, there are two clear upwelling centers, at 13ºN and 24ºN, with minimum values of -
296 0.36 ºC/decade. In these upwelling centers, the negative trends are lower than in the open ocean at the
297 same latitudes.

298 Finally, in the BeUS (Fig 3d), the mean trend is 0.19 (SD= 0.09) ºC/decade, closer to the average of the
299 CanUS. The two warm fronts with trends over 0.40 ºC/decade can be found in both the north and south
300 ends. In the round-year upwelling area, the Lüderitz cell (Andrews and Hutchings, 1980; Lutjeharms and
301 Meeuwis, 1987; Peard, 2007), the minimum value is -0.25 ºC/decade. In contrast, for the open ocean area
302 between the two warm fronts, the values are similar to those found in the CanUS (Fig 3b), around 0.20
303 ºC/decade.

304 The average trend for each region reveals higher open ocean warmings for the Atlantic EBUS (0.20 and
305 0.19 ºC/decade for the CanUS and BeUS, respectively) than the Pacific Ocean (0.10 and 0.007 ºC/decade,
306 for the CalUS and HuUS, respectively), with the lower trends observed in the HuUS. However, the trends
307 along the coast are rather heterogeneous, responding to the variability of the local upwelling dynamics,

308 as seen in Fig 3, where several permanent upwelling centers (negative trends) exist along the coast on

309 both continents.

a) SST Trends of CalUS
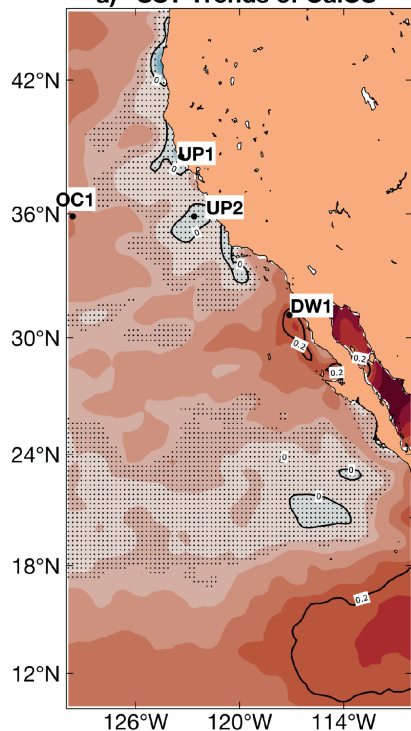
b) SST Trends of CanUS
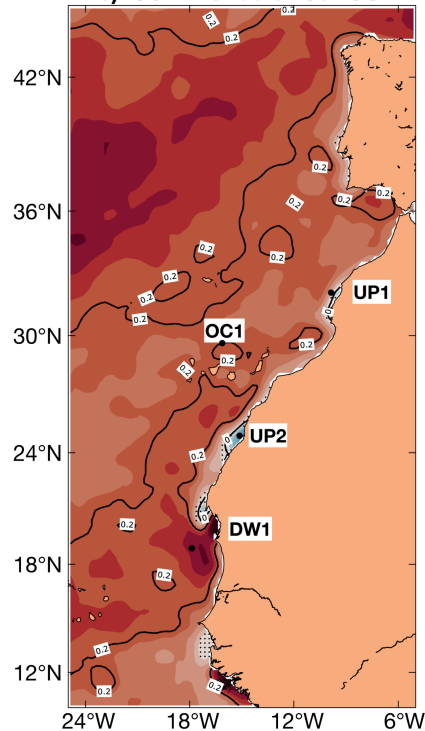
c) SST Trends of HuUS
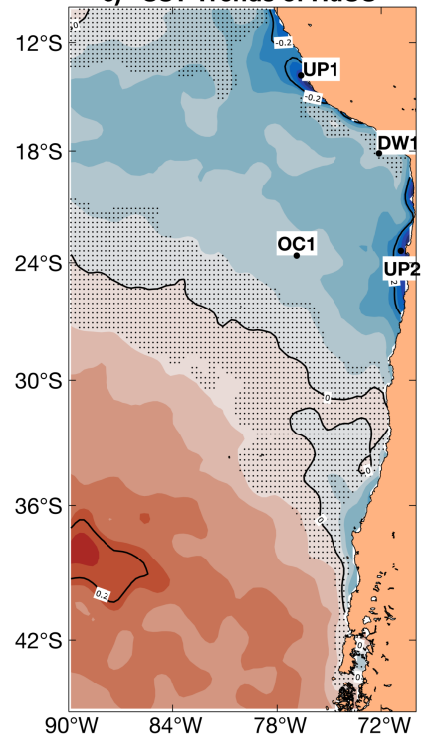
d) SST Trends of BeUS
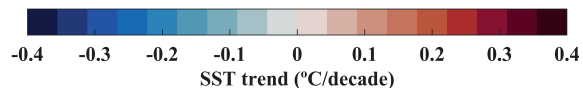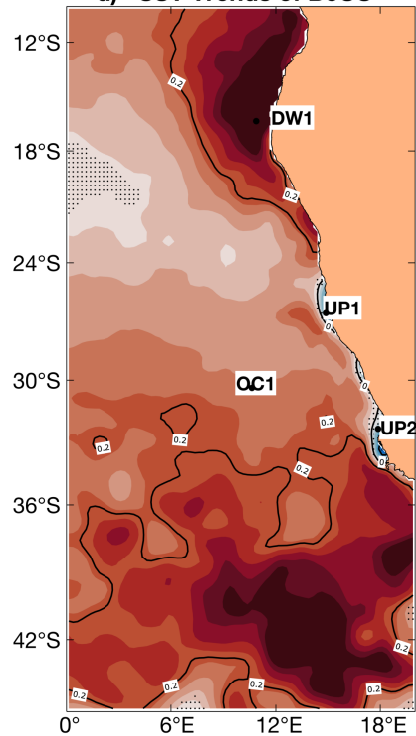
SST trend (ºC/decade)

Fig 3: Mapped SST trends (ºC/decade) for the major EBUS: a) California -CalUS, b) Canary-CanUS, c) Humboldt-HuUS, and d) Benguela-BeUS. The color scale indicates the trend values at the right margin of each graph. Black-dots shaded areas indicate non-significant trends. The locations of the areas selected (UP1, UP2, OC1, and DW1) are marked with solid black circles and labelled with their names. Black contours enclosed the isotrends -0.20, 0, and 0.20°C/decade.

310 **4.3. Trends in the upwelling cells and open ocean areas.**

311 Although we got an overview of the long-term trends for each EBUS in the previous section, the

312 validation of Bakun's hypothesis would require a finer resolution to describe the local dynamics of the

313 upwelling and identify those areas where the coastal upwelling is the main forcing. In this sense, we have

314 chosen representative points (see criteria in Section 3.4 and Figs 2 and 3) of both EBUS and non-EBUS

315 areas instead of using the large-averaged regions shown in Fig 3. These upwelling points are the upwelling

316 centers (UP1, UP2), the nearshore areas where the upwelling is not the primary process (DW1), and the

317 open ocean areas (OC1).

318 The CalUS presents the weakest trends of all the EBUS in both year-round upwelling centers, being -0.06

319 ºC/decade for UP1 and non-significant in UP2 (-0.03 ºC/decade, Fig 4a). For the open ocean area, the

320 OC1 trend is positive with a value of 0.14 ºC/decade, a lower value than the trend of 0.22º C/decade of

321 the DW1. On the Atlantic, the CanUS (Fig 4b) possesses the only positive trend (0.07 ºC/decade) of all

322 the EBUS in an upwelling area (UP1). Despite UP1 being positive, the trend is closer to zero than in the

323 OC1 (0.20 ºC/decade). Furthermore, the UP2 cell in the CanUS shows a trend twice as negative (-0.15

324 ºC/decade) as the one on the CalUS upwelling UP1. The OC1 and DW1 areas show a warmer trend in the

325 CanUS than in the North Pacific region (Fig 4). All of the above suggests that on the Northern Hemisphere

326 EBUS, Bakun's hypothesis is fulfilled, and this is even more significant in the CanUS despite having been

327 dismissed in previous studies (Sydeman et al., 2014).

328 In the HuUS (Fig 4c), we find a different behavior than the one seen on the other EBUS, showing negative

329 trends in all the representative locations. The upwelling centers of the HuUS present the greatest cooling

330 trend of all the EBUS, -0.30 ºC/decade at UP1 and -0.26 ºC/decade at UP2. As observed in CanUS, the

331 values for HuUS in OC1 (0.06 ºC/decade) are similar to the ones of DW1, although DW1 is non-

332 significant in the HuUS. Its counterpart in the Atlantic Ocean, the BeUS (Fig 3d), presents significant

333 large negative trends in the year-round upwelling areas (-0.23 ºC/decade for UP1 and -0.10 ºC/decade for

334 the UP2) and positive trends in OC1, 0.14 ºC/decade. The trend of the DW1 is the warmest (0.57
335 ºC/decade) found in all the EBUS, and it is related to the warm inflow from the Indian Ocean.
336 Overall, the trends show warming in the OC1 areas while cooling in the upwelling areas, except for the
337 HuUS, where the trend at the OC1 is also slightly negative. The contrast between the trends of upwelling
338 and open ocean areas found throughout the EBUS indicates upwelling intensification. To quantify this
339 intensification, it is necessary to have an index that compares the intensification of the upwelling with the
340 global warming trend on the open ocean area, that can be compared for all the EBUS. To compare the
341 intensification between upwellings and to further understand the impact of the oceanic background on
342 these trends, we will use the index α_{UI} described before to normalize the trends of each EBUS.

b) CanUS

SST (°C)

UP1
0.07* ± 0.04

UP2
-0.15* ± 0.05

OC1
0.29* ± 0.05

DW1
0.20* ± 0.04
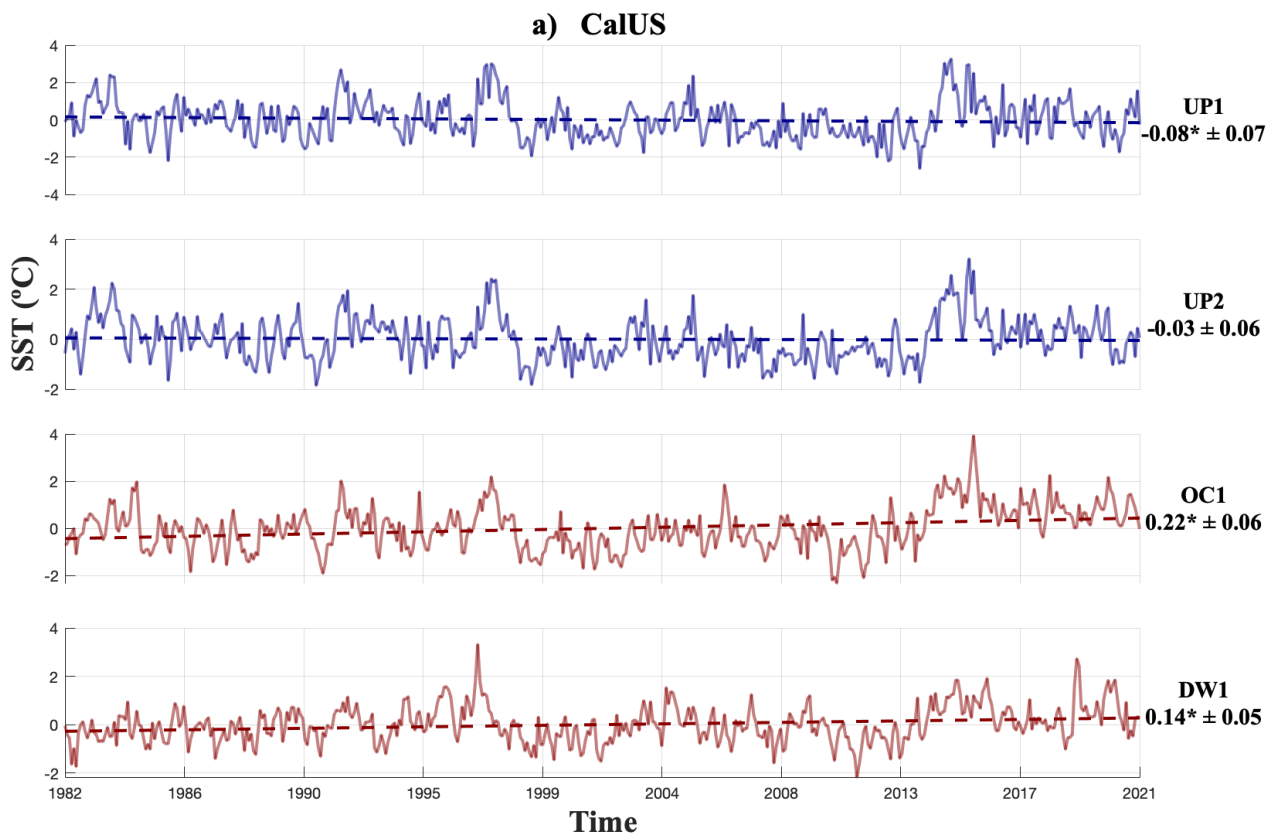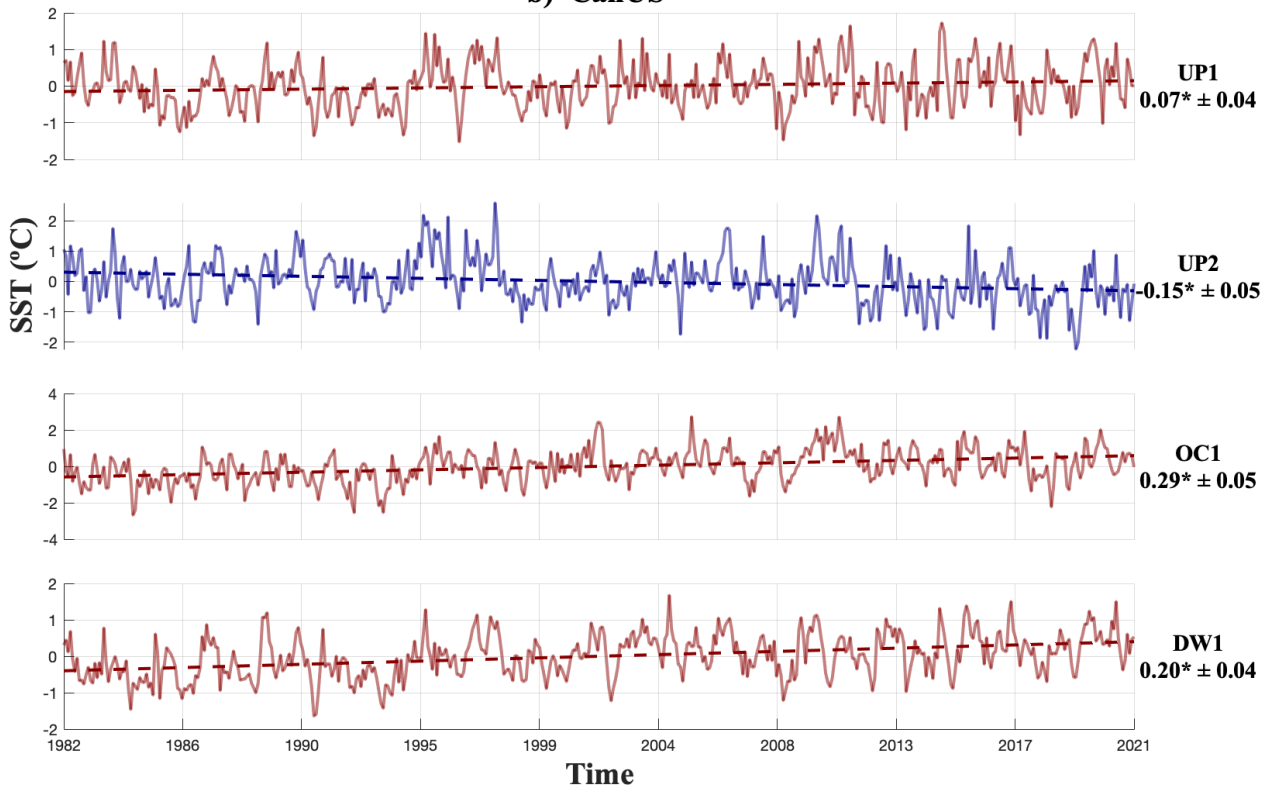
Time

c) HuS
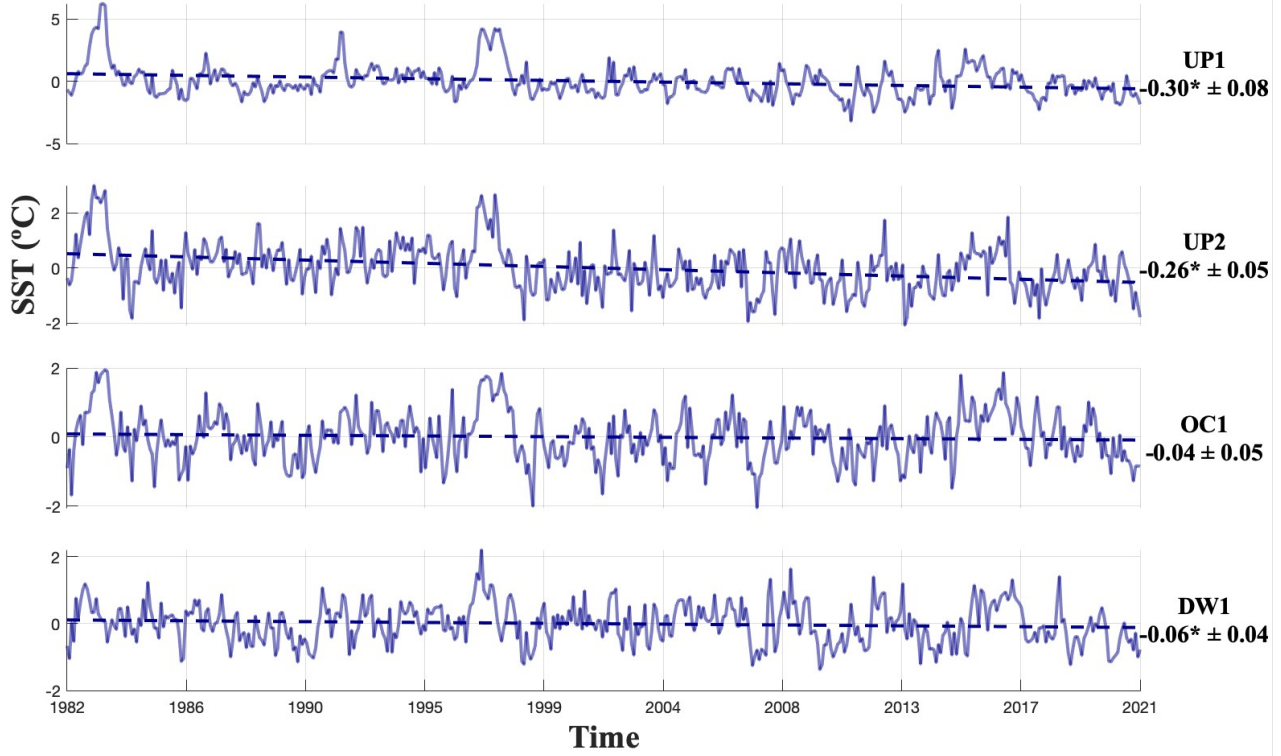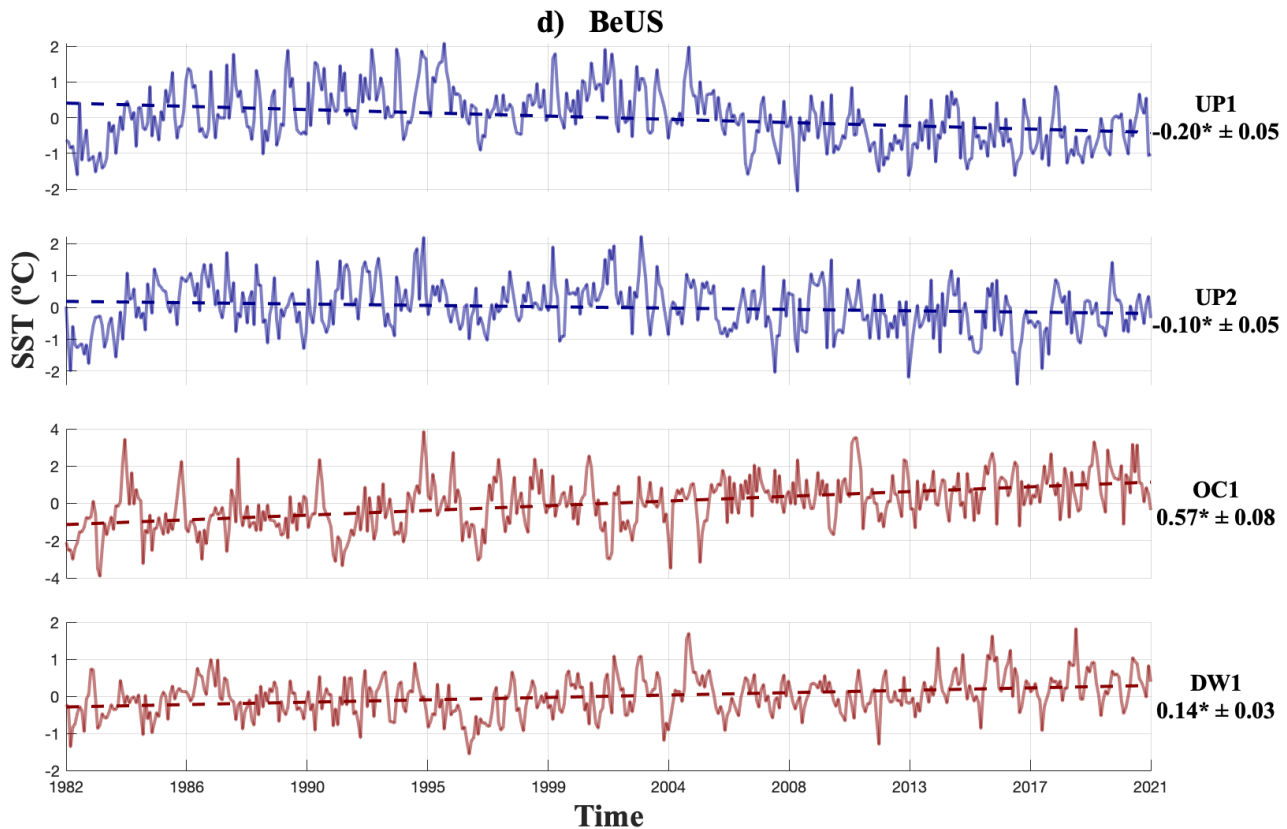
Fig 4: SST time series and trends (ºC/decade) for the selected areas for each one of the EBUS (DW1, UP1, and UP2) and the areas representative of the open ocean (OC1) in each EBUS: a) California, b) Canary, c) Humboldt and d) Benguela. The blue lines are for negative (cooling) trends, and the red ones are for positive (warming) trends. On the right side of the Y-axis, the trends are shown in ºC/decade, along with the area's label and confidence interval. Mann-Kendall significant trends (p-value<0.05) are resalted with the symbol "*" next to their value.

343 **4.4. The relation between Oceanic and EBUS trends.**

344 Global warming induces the increase of oceanic SST, and under Bakun's hypothesis, it also enhances the

345 favorable upwelling winds responsible for intensifying the upwelling areas. We define an angle between

346 the upwelling and oceanic trends, as described in the methodology section, to discern Bakun's hypothesis

347 from the global increase in SST. As described previously (Fig 4), the upwelling centers UP1 (except for

348 the CanUS, where UP2 will be used due to the warming detected on UP1 in Section 4.3) have the strongest

349 cooling, and we will use these trends (hereafter, in this section UP) to create the angle contrasts with the

350 positive warming trend of the open ocean (OC1) area for each EBUS (Fig 4).

351 For CanUS, the α_{UI} obtained between the UP and OC1 trends is 20º± 2º whereas it is 11º±3º in the CalUS,

352 21º±2º for the BeUS, and 14º±3º for the HuUS. The smallest angle is found in the CalUS because of the

353 low cooling and warming trends described in Section 4.3. This result for the CalUS is coherent with the

354 overall non-significant trends in the Mann-Kendall test (Fig 3a). The BeUS and CanUS have the highest

355 contrast between the two regression lines (recall that we observed similar UP and OC1 trends in the

356 Atlantic Ocean in Section 4.3) presenting similar α_{UI}.

357 The BeUS and CanUS show a weaker negative trend than the HuUS, but the oceanic background at the

358 HuUS leads to a smaller angle. At the HuUS, a negative SST trend is observed for the whole study area.

359 The hypotheses existing suggest that this trend is led either by a stronger La Niña (Meehl et al., 2016) or

360 related to the Southern Ocean SST changes (Kang et al., 2023b, a). Nevertheless, at the HuUS, we have

361 the most prominent upwelling negative trend. However, when normalized with the open ocean trend, the

362 Bakun's effect is reduced. In the annual upwelling series of CalUS and HuUS, there are two prominent

363 peaks associated with El Niño appeared around 1983 and 1997.

364 In general, we found positive α_{UI} for all the EBUS, supporting the intensification of the upwelling-oceanic

365 gradient, as expected from Bakun's hypothesis.
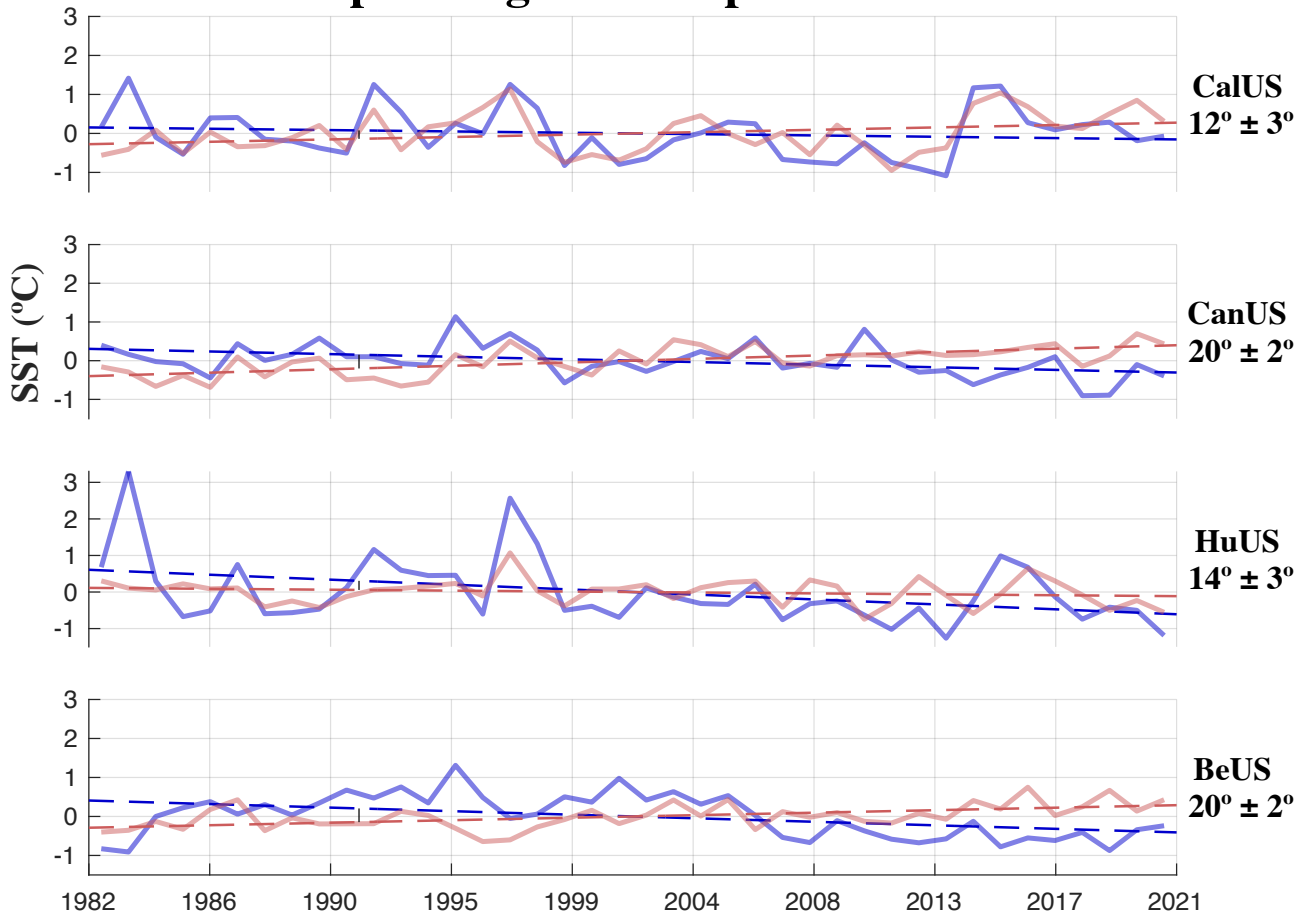
Fig. 5: EBUS SST trends (ºC/decade) against non-EBUS areas trends for each region. The EBUS annual series (continuous line) and trend (dotted line) are shown in blue; the same is true for the non-EBUS but is represented in red. On the opposite side of the Y-axis is labelled the α_UI with their corresponding EBUS.

4.5. Latitudinal distribution of α_UI

Many authors have previously tested the Bakun hypothesis, providing little consensus on both historical and projected records (Barton et al., 2013; Belkin, 2009; McGregor et al., 2007; Sambe et al., 2016, and Sydeman et al, 2014;). Such controversy has yielded alternative hypotheses to explain changes observed in the magnitude and timing of upwelling processes. Rykaczewski et al. (2015), suggests an alternative mechanism to the intensification of the upwelling process. They suggest a poleward shift of the oceanic high-pressure system which would stimulate latitude-dependent changes in the upwelling winds. To

address this, we have calculated the latitudinal distribution of the α_{UI} (see Fig 6) in each EBUS. The spatial variability of the upwelling intensity proxy, α_{UI}, reveals distinct patterns and regional differences. In the CalUS, upwelling intensification demonstrates consistent upwelling activity between 35°N to 45°N with αUI values reaching up to approximately 10° (Fig 6a). Conversely, in the CanUS, significant upwelling intensification is observed between 20°N and 30°N, with α_{UI} values peaking at 20º and in locations consistent with our dynamical analysis based on literature review (Fig 2b, UP1 and UP2). Similarly, in the HuUS upwelling intensification is confined to low latitudes (10-20 ºS, Fig 6c), and the values are close to those of the CalUS, (index values around 10º), as seen in the previous section. In contrast with the other regions, the BeUS shows intensification at high latitudes with maximum values of α_{UI} (20º) in the upwelling center of this region – Lüderitz upwelling center at 25ºS and Cape Columbine (around 32ºS)-. While results of BenUS and CalUS appear consistent with the findings by Rykaczewski et al, (2015), there is no supportive evidence in the other regions. To elucidate the possible mechanism responsible for such differences we will attend to the driver of the favorable-upwelling wind, the sea level pressure gradient
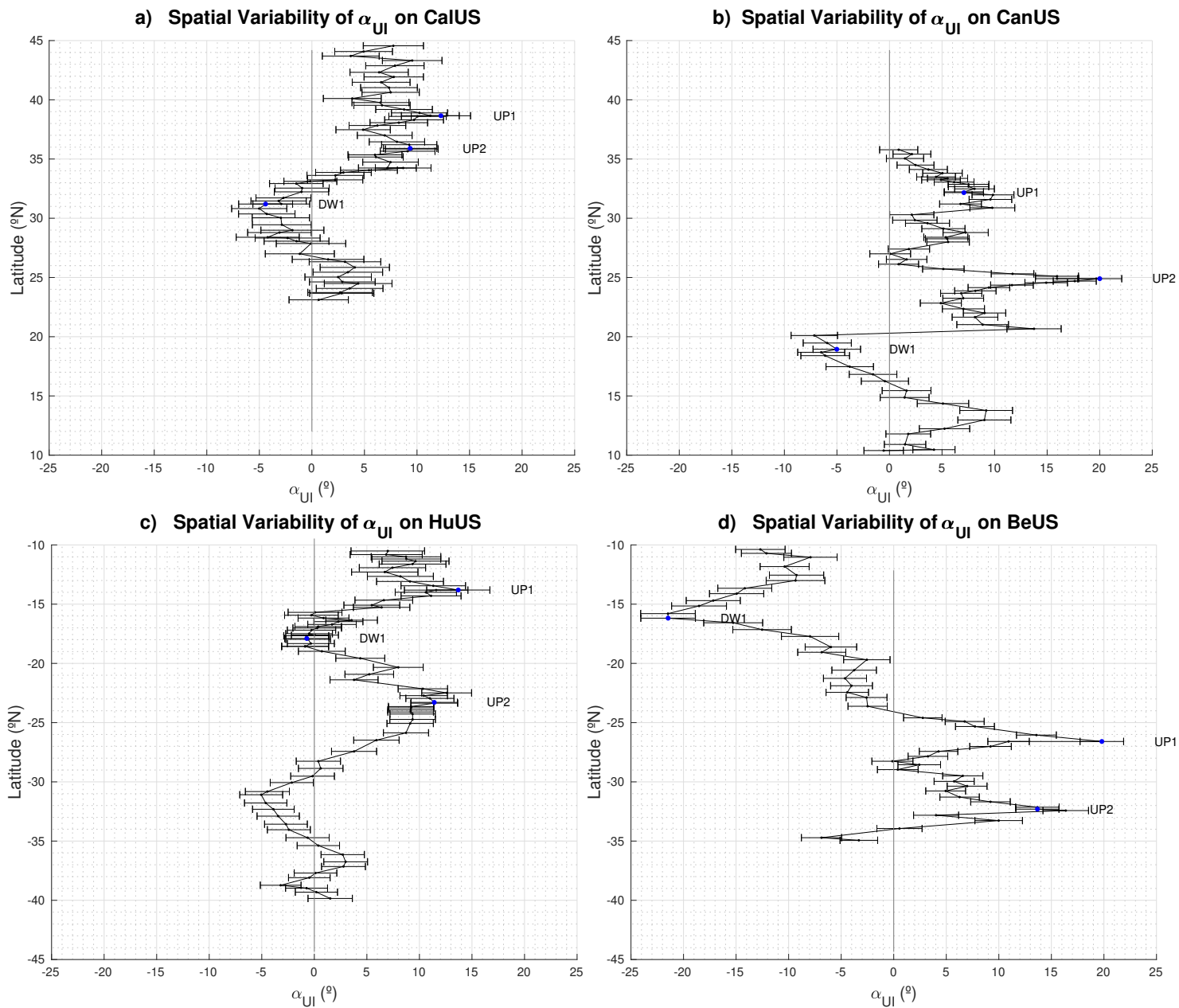
Fig 6: Spatial distribution of the α_UI (over the period of 1982-2021) along the coast for CalUS (a), CanUS (b), HuUS(c) and BeUS(c). The α_UI is calculated between grid points along the coast and OC1.

387 **4.6. SLP Gradients**

388 The coastal upwelling intensification postulated by Bakun mechanism, in 1990, would involve a stronger
389 increase of near-surface temperature over land than over the ocean, which would lead to an intensification
390 of the continental thermal low-pressure system relative to the ocean. To test this driver mechanism, we
391 have calculated the trends (Fig 7) of the gradient between the continental thermal low and the oceanic
392 high pressure.
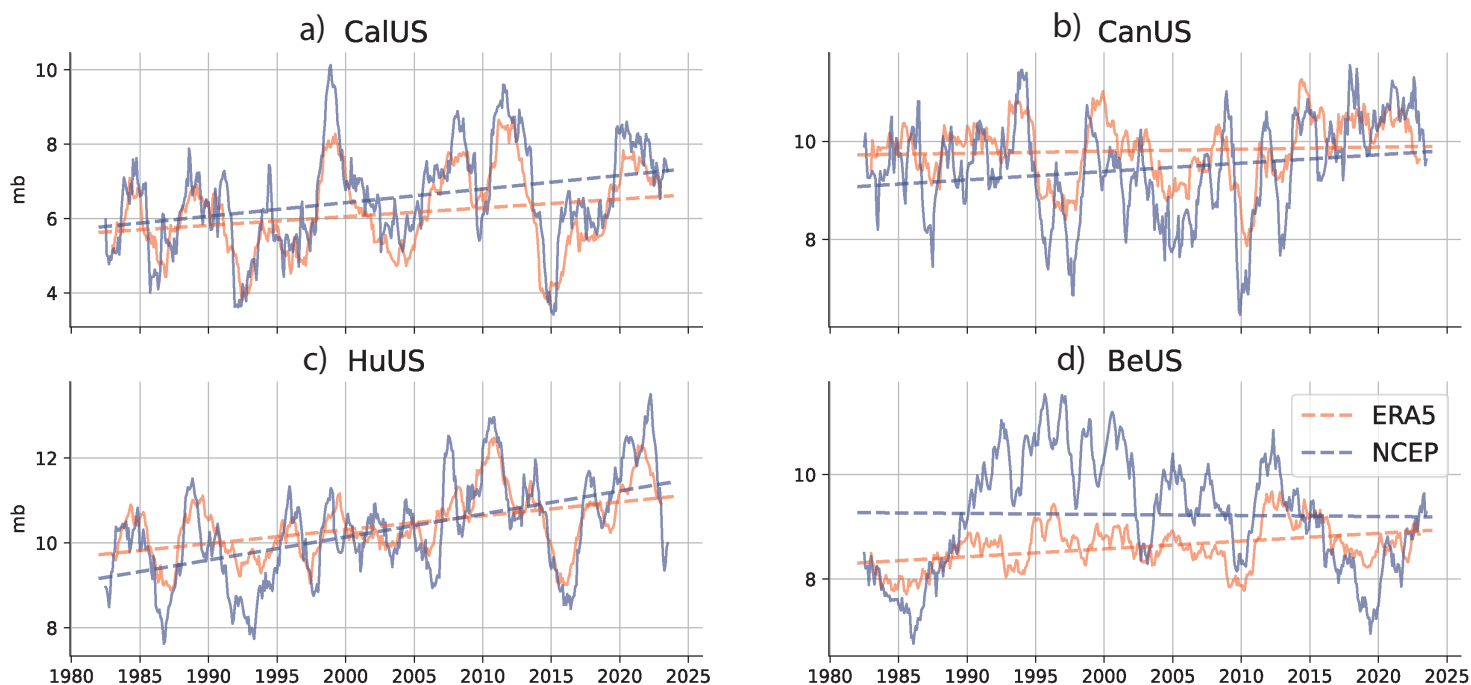
Fig 7: EBUS SLP gradients trends and temporal series for NCEP (blue lines) and ERA5 (red lines) datasets over the period 1982- 2023.

393 For ERA5, we found positive and significant trends (see Table 3) for all Eastern Boundary Upwelling
394 Systems (EBUS). Specifically, the trends in SLP gradients are 0.24 mb/decade (0.039) for CalUS, 0.04
395 mb/decade (0.017) for CanUS, 0.33 mb/decade (0.038) for HuUS, and 0.015 mb/decade (0.051) for
396 BeUS. On the other hand, the NCEP dataset shows no significant trend for the BeUS but stronger trends
397 than ERA5 for the other EBUS, with 0.37 mb/decade (0.073) for CalUS, 0.17 mb/decade (0.034) for
398 CanUS, 0.54 mb/decade (0.070) for HuUS, and -0.02 mb/decade (0.072) for BeUS. However, due to its

coarser resolution (2º) compared to ERA5 (0.25º), NCEP data is arguably less reliable. Nevertheless, these results support an intensification of the pressure gradient.

	CalUS (mb/decade)	CanUS (mb/ decade)	HuUS (mb/ decade)	BeUS (mb/ decade)
ERA5	0.24 (0.039)	0.04 (0.017)	0.33 (0.038)	0.015 (0.051)
NCEP	0.37 (0.073)	0.17 (0.034)	0.54 (0.070)	-0.02 (0.072)

Table 3. Values of the trend, over the period 1982-2023, for the ERA5 (first row) and NCEP (second row) for all the EBUS. Parentheses enclose spatial standard deviation.

5 Discussion and Conclusions.

The future of the EBUS under global warming conditions remains uncertain. The controversies around Bakun's hypothesis -an intensification of the upwelling due to the increase of the continental low-pressure system driven by global warming- have its source in (1) discrepancies between wind stress datasets and (2) differences in the methodologies used.

On one hand, Barton et al. (2013) highlighted a lack of consensus among various wind datasets, since they did not observe statistically significant changes in the meridional (upwelling-favorable) wind. These discrepancies in wind data are consistent with those noted by Narayan et al. (2010), who, despite finding significantly increasing in coastal upwelling areas when using COADS wind stress, also found that the NCEP/NCAR wind stress indicated a significant decrease in the upwelling off NW Africa, and a non-statistically significant trend for Lüderitz, California, and the Peruvian upwelling areas. Furthermore, they also observed that the ERA-40 dataset showed an increasing coastal upwelling in the NW African and Peruvian upwelling areas but a decreasing in the California upwelling areas, with a non-statistically significant trend in the Lüderitz upwelling areas Therefore, using wind data as a proxy for upwelling leads to a wide spread of results as it strongly depends on the data product used.

On the other hand, SST-based indexes are usually constructed from thermal differences between coastal and offshore SST areas taken at the same latitude and following the coastline (Benazzouz et al., 2014; Gómez-Gesteira et al., 2008; Santos et al., 2012). This methodology does not consider the regional upwelling dynamics, and average upwelling centers with areas without upwelling. Abrahams et al. (2021) introduced an upwelling metric based on marine heatwave detection techniques, examining favorable

upwelling winds and SST data together. Their findings revealed a strong association between a decrease in SST and an increase in upwelling intensity. Their novel methodology holds significant importance in unraveling the connection between the physical upwelling phenomenon and its ecological impacts. However, predicting ecological impacts remains challenging. While intensified upwelling could mitigate habitat warming, it may also increase ocean acidification, hypoxic events and reduce suitable food for fish larvae (Abrahams et al., 2021; Bakun et al., 2015). Nonetheless, they successfully establish a link between decreased SST and changes in upwelling intensity, even when trends in wind dynamics do not fully account for the upwelling response, reinforcing the notion that SST is a suitable proxy for upwelling intensity. However, their SST metrics exhibited inconsistencies across upwelling areas, except for the Humboldt system. These inconsistencies may be due to the averaging of data across extensive areas, mixing upwelling areas with areas without the associated cold water of upwelling. Abrahams et al. (2021) also explored these metrics in upwelling-favorable winds data, and their results indicated that decadal trends were generally not significant. As previously discussed, wind products often yield contradictory results despite their direct relevance to upwelling. Hence, our study complements Abrahams et al. (2021) since we have focused on SST to understand longer terms changes in the upwelling intensity, using areas with optimal signal-to-noise ratio, namely the upwelling centers, revealing upwelling-related cool water in all Eastern Boundary Upwelling Systems (EBUS).

Therefore, in this study, we assess the intensification of the upwelling from a regional perspective, by using SST trends at locations representative of upwelling and of an open oceanic reference location for each different EBUS.

Additionally, we tested the effects of averaging areas on the index (see supplementary material, Fig S4 and Table S1). Our findings indicate that the averaged response is influenced by the dynamical regions involved, rather than by the size of the region averaged. This is evidenced by the invariant results when including the three coastal areas (DW1, UP1 and UP2). In contrast, focusing on specific upwelling zones, particularly around upwelling centers, made the intensification more evident. Moreover, we verified the stability of the trend both spatially and temporally by performing the analysis of Barton et al. (2013) across all the EBUS (supplementary material, Fig S5).

450 Furthermore, to assess the strength of the net upwelling intensification, we proposed an index that allows

451 inter-basin comparisons attending to their regional background. SST, often used as an indicator of coastal

452 upwelling, can be influenced by various factors, such as changes in surface mixing and offshore storm

453 activity. However, in our long-term analysis of monthly and deseasonalized SST records, the seasonal

454 and synoptic processes have minimal influence on the SST-upwelling intensity relationship. Moreover,

455 Wang et al. (2015) explored the connection between sea-land thermal gradients and offshore Ekman

456 transport using the CMIP5 models. Their findings underscore the significant link between thermal

457 gradients and offshore Ekman transport, even under greenhouse gas emission scenarios. McGregor et al.

458 (2007) and Santos et al. (2012) also support this relationship, emphasizing significant correlations

459 between coastal SST and offshore Ekman transport, reinforcing the utility of coastal SST as a proxy for

460 assessing upwelling intensity.

461 To assess the quality of our results, we validated the NOAA SST reanalysis with in-situ data from both

462 the Atlantic and Pacific Oceans before estimating the trends in all EBUS. Overall, the Atlantic Ocean had

463 lower correlations with the satellite data than the Pacific Ocean, likely due to shorter in-situ records.

464 Nevertheless, we found high and robust correlation coefficients (>0.7) that sustain the satellite SST trends

465 in oceanic and upwelling areas. We observed negative SST trends in all the EBUS, being stronger in the

466 southern hemisphere (the strongest located in the HuUS-UP1 showing a -0.30ºC/decade) than in the

467 northern hemisphere (the weakest in the CalUS-UP2 with a trend of -0.06ºC/decade). Our results are

468 consistent with the meta-analysis by Sydeman et al. (2014), who concluded that a significant

469 intensification of upwelling exists from observational and model data, except for the case of CanUS.

470 Other studies have investigated the SST trends in the EBUS but with an approach that did not consider

471 the heterogeneity of the upwelling areas. For instance, in the CalUS, Seabra et al. (2019) reported a

472 0.06ºC/decade warming rate, over the period 1982–2018. However, their approach involved averaging a

473 500 km nearshore area, excluding non-significant regions. Thus, almost half of the extension was not

474 considered, resulting in the average of different dynamical areas and the exclusion of upwelling centers.

475 Belkin et al. (2009) performed a similar analysis but included the entire CalUS nearshore area. They found

476 a net change of -0.035 ºC/decade over the 1982-2007 period, agreeing in sign with our study but showing

477 a higher (more positive) rate due to the use of a large average. In contrast, Siemer et al. (2021) found

478 negative trends of -0.14ºC/decade, over the period 1982-2019, for the CanUS permanent upwelling area,

479 like our results (-0.15ºC/decade). However, this trend fades away and becomes positive when they

480 average the whole coastal upwelling area, highlighting the relevance of the methodology used in this

481 study. Likewise, many studies carried out in this area present positive trends for the upwelling due to the

482 method used (Belkin, 2009; Demarcq, 2009; Seabra et al., 2019). In line with our study, Seabra et al.

483 (2019) found the coolest trends (-0.07 ± 0.08°C/decade) in the HuUS. However, like in other EBUS, using

484 average areas increased the trend values. This pattern is also observed by Belkin et al. (2009), where the

485 net change of the average nearshore area results in -0.05ºC/decade. For the BeUS, similar to CanUS,

486 averaging the entire coastal upwelling area results in the fading of the observed upwelling trend. Hence,

487 a warming rate of 0.17 ºC/decade is found in Seabra et al. (2019). In contrast, Santos et al. (2012)

488 investigated trends, over the period 1982-2010, close to the shore without averaging areas and found a

489 negative trend of the BeUS, strongly agreeing with our results (-0.13 ºC/decade). Hence, a warming rate

490 of 0.17 ºC/decade is found in Seabra et al. (2019). In contrast, Santos et al. (2012) investigated trends

491 close to the shore without averaging areas and found a negative trend of the BeUS, strongly agreeing with

492 our results (-0.13 ºC/decade).

493 While all the upwelling trends are negative and support the Bakun's hypothesis, the oceanic trends behave

494 differently across basins. We observed warming in all the open ocean areas except in the HuUS, where a

495 cooling of –0.06ºC/decade is observed. Dong & Zhou (2014) studied the influence of the Interdecadal

496 Pacific Oscillation (IPO) on Global Warming trends. Their EOF analysis results indicate that the transition

497 to the negative phase of the IPO modes is responsible for the cooling trends observed in the Pacific.

498 The warming in the CalUS and BeUS is 0.14ºC/decade (over the period 1982-2023), while this trend is

499 slightly more prominent in the CanUS. Seabra et al. (2019) revealed oceanic warming rates

500 (0.06ºC/decade), over the period 1982–2018, on the averaged upwelling in CalUS lower than the OC1

501 trend (0.14ºC/decade). The open ocean positive trend of the CanUS is identical to the one in Siemer et al.

502 (2021) and further agrees with other studies (Belkin, 2009; Good et al., 2007; Signorini et al., 2015). The

503 result of Seabra et al. (2019) in HuUS also showed a very similar trend (-0.07 ºC) compared with our OC1

504 trend. Finally, in the BeUS, a good agreement is found with the average warming rate of Seabra et al.

505 (2019). Our study demonstrates good agreement with existing literature on oceanic trends despite the

506 differences in methodologies employed. Our study demonstrates good agreement with existing literature

507 on oceanic trends despite the differences in methodologies employed.

508 Although long-term changes, such as the North Atlantic Oscillation or the Pacific Oscillation, can impact

509 the SST gradient, their effect would not surpass the ability of our analysis to support Bakun's hypothesis.

510 In that sense, Nayaran et al. (2010) found that correlations between upwelling indices and climate indices

511 like the Atlantic Multidecadal Oscillation Index (AMOI) lack significance. Similarly, the North Atlantic

512 Oscillation Index (NAOI) exhibits a notable negative correlation with meridional wind stress off NW

513 Africa, yet its correlation with the SST index remains insignificant. In the case of the CalUS, the Pacific

514 Decadal Oscillation Index (PDOI) shows a weak but statistically significant correlation with the coastal

515 upwelling SST index off California. However, no substantial correlation is found with alongshore wind

516 stress. Cross-correlation analyses also reveal a lack of significant correlations across various time lags.

517 On the other hand, (Bonino et al., 2019) found that local drivers and trends favoring upwelling (e.g.,

518 equatorward wind stress, cyclonic wind stress curl, and thermocline depth variation) explain the low-

519 frequency modulation of upwelling. Bonino et al. (2019) also explored the link between wind-based

520 upwelling indices and climate modes. They found that Atlantic and Pacific upwelling variabilities are

521 mainly independent, while intra-basin domain variabilities present some coherency, which is consistent

522 with our results. This intra-basin covariability is especially marked in the Pacific Ocean, where the shared

523 variability is majorly due to the El Niño Southern Oscillation (ENSO) mode. In contrast, in the Atlantic

524 Ocean, coherent variability is associated with upwelling trends, whereas only in the CanUS is it linked to

525 the AMO. These results suggest that long-term climate indices may influence coastal upwelling dynamics,

526 which is especially important in the Pacific. However, our index, $\alpha_{UI,}$ by normalizing the trend for its

527 oceanic background, our results should account for the effects of local climate indices.

528 To assess Bakun's hypothesis and, thus, the upwelling capacity to overcome the oceanic warming effect,

529 we define the angle ($\alpha_{UI,}$ readers are referred to section 3.3) between oceanic water and upwelling trends.

530 Because this new index is directly based on trends, it captures only the low-frequency variability.

531 Additionally, we verified the method's robustness using a probabilistic assessment of the uncertainties

532 that showed consistent intensifications for all EBUS (Fig 5). This new approach differs from the

traditional trend analysis since it normalizes the upwelling trends by comparing them with open ocean changes.

The EBUS in the Pacific Ocean yields minimum α_{UI} ($10°\pm3°$ and $14°\pm3°$ for CalUS and HuUS, respectively), which is consistent with the low signal-to-noise ratio of global warming on this ocean, given its natural variability. The overall cooling signal caused by the IPO enhances the HuUS open ocean negative trends. Still, our index normalizes the upwelling trend to the full basin variability, suggesting the possibility of a mild Bakun effect even at the HuUS. In the Atlantic Ocean, the α_{UI} for the CanUS and BeUS are $20°\pm2°$ and $21°\pm2°$, respectively, twice as large as on the Pacific Ocean. The α_{UI} presents wider angles at the southern hemisphere EBUS than in the northern hemisphere EBUS. Nevertheless, our results show a significant difference between oceanic and coastal trends reflected in positive α_{UI} in all EBUS (Fig 5).

The SST changes in the EBUS respond mainly to changes in the upwelling processes which are ultimately driven by the pressure gradients. We analyzed the pressure gradients trends in all four EBUS. Our findings further support the intensification of the pressure gradients driven by climate change, as stated by Bakun (1990). However, there are probably other contributors to the intensification of the upwellings. Some researchers question whether the impacts of differential heating on the pressure gradient force drives intensification of coastal upwelling. Rather, a complementary hypothesis proposes that evidence of an intensifying pressure gradient force is limited to poleward migration of the Hadley Cell (Arellano and Rivas, 2019; Rykaczewski et al., 2015; Wang et al., 2015). Nevertheless, these projections are only supported by observational records in the Humboldt and Benguela Systems, (Sydeman et al., 2014). In contrast, we have tested this hypothesis on the historical record by computing the latitudinal distribution of α_{UI}. The results shown in Fig 6 partially agree with Rykaczewski et al, (2015), as only CalUS and BeUS presented a poleward intensification of α_{UI}. To further understand the drivers of these changes, we examined the spatial stability of the trends in the SLP continental-oceanic gradient was also tested using Monte Carlo simulation. The discrepancy between the latitudinal distribution of α_{UI} and the small standard deviation of trends around the cores of the pressure systems suggests that the hypothesis of poleward displacement of the high-pressure systems remains inconclusive.

560 In summary, in this study, we use SST at discrete locations and the pressure gradient to explore the
561 Bakun's hypothesis in the four major EBUS. Cooling trends are observed for all upwelling areas (the
562 strongest in the HuUS and the weakest in the CalUS), and mainly warming trends offshore except for the
563 HuUS. In addition, a novel index α_{UI} that normalizes the upwelling trends to their background open ocean
564 trend is proposed. This index is easy to estimate, allows interbasin trend comparisons, and helps
565 understand the role of changing upwellings in a changing climate. The index reveals that the Bakun
566 hypothesis remains a possible mechanism for upwelling intensification in all four EBUS, although the
567 Atlantic Basin shows a higher intensification effect than the Pacific Ocean, and slightly stronger in the
568 southern hemisphere than in the northern hemisphere.

569 **Data availability.**

570 The moored data analyzed in this study are available
571 at https://www.ndbc.noaa.gov/ and https://www.puertos.es/es-es/oceanografia/Paginas/portus.aspx for
572 the Pacific and Atlantic Ocean, respectively. The cruise data are also available
573 at https://calcofi.org/data/ for the Pacific Ocean and upon request from the author in the case of the
574 Atlantic Ocean. And for the Satellite-based SST data, the NOAA reanalysis product
575 are avalaible from https://www.ncei.noaa.gov/data/sea-surface-temperature-optimum-
576 interpolation/access/avhrr-only/.

577 **Author contribution**

578 M, Gutierrez-Guerra processed the data, and carried out all data analyses. M, Gutierrez-Guerra wrote the
579 original paper with contributions from M, Gutierrez-Guerra, M.D, Perez-Hernandez and P, Velez. M.D,
580 Perez-Hernandez and P, Velez supervised the study. All authors reviewed and edited the final paper.

581 **Competing interests**

582 The contact author has declared that none of the authors has any competing interest.

583 **Acknowledges**

584 This article is a publication of the Unidad Océano y Clima from Universidad de Las Palmas de Gran
585 Canaria, an R&D&I CSIC-associate unit. This work has been completed as part of the doctoral program
586 in Oceanography and Global Change at the Instituto de Oceanografía y Cambio Global (IOCAG). M.A.
587 Gutiérrez-Guerra acknowledges the Agencia Canaria de Investigación, Innovación y Sociedad de la
588 Información (ACIISI) and the Fondo Social Europeo Plus (FSE+) Programa Operativo Integrado de
589 Canarias 2021-2027, Eje 3 Tema Prioritario 74 (85%) grant program of "Apoyo al personal investigador en
590 formación" FPI2024010234 and the INVESTIGO grant program of "Plan de Recuperación, Transformación
591 y Resiliencia – Next Generation EU".

592 **References**

593 Abbott, M. R. and Zion, P. M.: Spatial and temporal variability of phytoplankton pigment off northern
594 California during Coastal Ocean Dynamics Experiment 1, J Geophys Res Oceans, 92, 1745–1755,
595 https://doi.org/10.1029/JC092IC02P01745, 1987.

596 Abrahams, A., Schlegel, R. W., and Smit, A. J.: Variation and Change of Upwelling Dynamics Detected
597 in the World's Eastern Boundary Upwelling Systems, Front Mar Sci, 8, 626411,
598 https://doi.org/10.3389/FMARS.2021.626411/BIBTEX, 2021.

599 Andrews, W. R. H. and Cram, D. L.: Combined Aerial and Shipboard Upwelling Study in the Benguela
600 Current, Nature 1969 224:5222, 224, 902–904, https://doi.org/10.1038/224902a0, 1969.

601 Andrews, W. R. H. and Hutchings, L.: Upwelling in the Southern Benguela Current, Prog Oceanogr, 9,
602 1–81, https://doi.org/10.1016/0079-6611(80)90015-4, 1980.

603 Arellano, B. and Rivas, D.: Coastal upwelling will intensify along the Baja California coast under
604 climate change by mid-21st century: Insights from a GCM-nested physical-NPZD coupled numerical
605 ocean model, Journal of Marine Systems, 199, 103207,
606 https://doi.org/10.1016/J.JMARSYS.2019.103207, 2019.

607 Bakun, A.: Global climate change and intensification of coastal ocean upwelling, Science (1979), 247,
608 198–201, https://doi.org/10.1126/science.247.4939.198, 1990.

609   Bakun, A. and Nelson, C. S.: The Seasonal Cycle of Wind-Stress Curl in Subtropical Eastern Boundary

610   Current Regions, J Phys Oceanogr, 21, 1815–1834, https://doi.org/https://doi.org/10.1175/1520-

611   0485(1991)021<1815:TSCOWS>2.0.CO;2, 1991.

612   Bakun, A., Black, B. A., Bograd, S. J., García-Reyes, M., Miller, A. J., Rykaczewski, R. R., and

613   Sydeman, W. J.: Anticipated Effects of Climate Change on Coastal Upwelling Ecosystems, Curr Clim

614   Change Rep, 1, 85–93, https://doi.org/10.1007/s40641-015-0008-4, 2015.

615   Bang, N. and Andrews, W.: Direct current measurements of a shelf-edge frontal jet in the southern

616   Benguela system, J Mar Res, 32, 1974.

617   Barton, E. D., Field, D. B., and Roy, C.: Canary current upwelling: More or less?, Prog Oceanogr, 116,

618   167–178, https://doi.org/10.1016/j.pocean.2013.07.007, 2013.

619   Belkin, I. M.: Rapid warming of Large Marine Ecosystems, Prog Oceanogr, 81, 207–213,

620   https://doi.org/10.1016/j.pocean.2009.04.011, 2009.

621   Benazzouz, A., Mordane, S., Orbi, A., Chagdali, M., Hilmi, K., Atillah, A., Lluís Pelegrí, J., and Hervé,

622   D.: An improved coastal upwelling index from sea surface temperature using satellite-based approach –

623   The case of the Canary Current upwelling system, Cont Shelf Res, 81, 38–54,

624   https://doi.org/10.1016/j.csr.2014.03.012, 2014.

625   Bonino, G., Di Lorenzo, E., Masina, S., and Iovino, D.: Interannual to decadal variability within and

626   across the major Eastern Boundary Upwelling Systems, Scientific Reports 2019 9:1, 9, 1–14,

627   https://doi.org/10.1038/s41598-019-56514-8, 2019.

628   Cropper, T. E., Hanna, E., and Bigg, G. R.: Spatial and temporal seasonal trends in coastal upwelling

629   off Northwest Africa, 1981–2012, Deep Sea Research Part I: Oceanographic Research Papers, 86, 94–

630   111, https://doi.org/10.1016/J.DSR.2014.01.007, 2014.

631   Demarcq, H.: Trends in primary production, sea surface temperature and wind in upwelling systems

632   (1998-2007), Prog Oceanogr, 83, 376–385, https://doi.org/10.1016/j.pocean.2009.07.022, 2009.

633   Dugdale, R. C. and Wilkerson, F. P.: New production in the upwelling center at Point Conception,

634   California: temporal and spatial patterns, Deep Sea Research Part A. Oceanographic Research Papers,

635   36, 985–1007, https://doi.org/10.1016/0198-0149(89)90074-5, 1989.

636 Ekman, V. W.: On the Influence of the Earth's Rotation on Ocean-Currents, Almqvist & Wiksells,

637 Uppsala [Sweden], 1–52 pp., 1905.

638 Escribano, R., Daneri, G., Farías, L., Gallardo, V. A., González, H. E., Gutiérrez, D., Lange, C. B.,

639 Morales, C. E., Pizarro, O., Ulloa, O., and Braun, M.: Biological and chemical consequences of the

640 1997–1998 El Niño in the Chilean coastal upwelling system: a synthesis, Deep Sea Research Part II:

641 Topical Studies in Oceanography, 51, 2389–2411, https://doi.org/10.1016/J.DSR2.2004.08.011, 2004.

642 Figueroa, D. and Moffat, C.: On the influence of topography in the induction of coastal upwelling along

643 the Chilean Coast, Geophys Res Lett, 27, 3905–3908, https://doi.org/10.1029/1999GL011302, 2000.

644 García-Reyes, M., Sydeman, W. J., Schoeman, D. S., Rykaczewski, R. R., Black, B. A., Smit, A. J., and

645 Bograd, S. J.: Under pressure: Climate change, upwelling, and eastern boundary upwelling ecosystems,

646 Front Mar Sci, 2, 1–10, https://doi.org/10.3389/fmars.2015.00109, 2015.

647 Gómez-Gesteira, M., De Castro, M., Álvarez, I., Lorenzo, M. N., Gesteira, J. L. G., and Crespo, A. J.

648 C.: Spatio-temporal upwelling trends along the Canary upwelling system (1967-2006), Ann N Y Acad

649 Sci, 1146, 320–337, https://doi.org/10.1196/annals.1446.004, 2008.

650 Good, S. A., Corlett, G. K., Remedios, J. J., Noyes, E. J., and Llewellyn-Jones, D. T.: The global trend

651 in sea surface temperature from 20 years of advanced very high resolution radiometer data, J Clim, 20,

652 1255–1264, https://doi.org/10.1175/JCLI4049.1, 2007.

653 Good, S. A., Martin, M. J., and Rayner, N. A.: EN4: Quality controlled ocean temperature and salinity

654 profiles and monthly objective analyses with uncertainty estimates, J Geophys Res Oceans, 118, 6704–

655 6716, https://doi.org/10.1002/2013JC009067, 2013.

656 Hutchings, L., van der Lingen, C. D., Shannon, L. J., Crawford, R. J. M., Verheye, H. M. S.,

657 Bartholomae, C. H., van der Plas, A. K., Louw, D., Kreiner, A., Ostrowski, M., Fidel, Q., Barlow, R.

658 G., Lamont, T., Coetzee, J., Shillington, F., Veitch, J., Currie, J. C., and Monteiro, P. M. S.: The

659 Benguela Current: An ecosystem of four components, Prog Oceanogr, 83, 15–32,

660 https://doi.org/10.1016/j.pocean.2009.07.046, 2009.

661 Kämpf, J. and Chapman, P.: Upwelling Systems of the World, https://doi.org/10.1007/978-3-319-

662 42524-5, 2016.

Kang, S. M., Yu, Y., Deser, C., Zhang, X., Kang, I. S., Lee, S. S., Rodgers, K. B., and Ceppi, P.: Global impacts of recent Southern Ocean cooling, Proc Natl Acad Sci U S A, 120, e2300881120, https://doi.org/10.1073/PNAS.2300881120/SUPPL_FILE/PNAS.2300881120.SAPP.PDF, 2023a.

Kang, S. M., Ceppi, P., Yu, Y., and Kang, I. S.: Recent global climate feedback controlled by Southern Ocean cooling, Nature Geoscience 2023 16:9, 16, 775–780, https://doi.org/10.1038/s41561-023-01256-6, 2023b.

Kendall, M.: Rank correlation methods (4th edn.) charles griffin, San Francisco, CA, 8, 875, 1975.

Lutjeharms, J. R. E. and Meeuwis, J. M.: The extent and variability of South-East Atlantic upwelling, South African Journal of Marine Science, 5, 51–62, https://doi.org/10.2989/025776187784522621, 1987.

Mann, H. B.: Nonparametric Tests Against Trend, Econometrica, 13, 245, https://doi.org/10.2307/1907187, 1945.

Marín, C.: Upwelling shadows at Mejillones Bay (northern Chilean coast): a remote sensing in situ analysis, Investigaciones Marinas, 31, 47–55, 2003.

McGregor, H. V., Dima, M., Fischer, H. W., and Mulitza, S.: Rapid 20th-century increase in coastal upwelling off northwest Africa, Science (1979), 315, 637–639, https://doi.org/10.1126/science.1134839, 2007.

Meehl, G. A., Hu, A., Santer, B. D., and Xie, S. P.: Contribution of the Interdecadal Pacific Oscillation to twentieth-century global surface temperature trends, Nature Climate Change 2016 6:11, 6, 1005–1008, https://doi.org/10.1038/nclimate3107, 2016.

Mesias, J. M., Matano, R. P., and Strub, P. T.: Dynamical analysis of the upwelling circulation off central Chile, J Geophys Res Oceans, 108, 3085, https://doi.org/10.1029/2001JC001135, 2003.

Narayan, N., Paul, A., Mulitza, S., and Schulz, M.: Trends in coastal upwelling intensity during the late 20th century, Ocean Science, 6, 815–823, https://doi.org/10.5194/OS-6-815-2010, 2010.

Pauly, D. and Christensen, V.: Primary production required to sustain global fisheries, Nature, 376, 279–279, https://doi.org/10.1038/376279b0, 1995.

Peard, K. R.: Seasonal and interannual variability of wind-driven upwelling at Lüderitz, Namibia, http://hdl.handle.net/11427/6498, 2007.

691 Reynolds, R. W., Smith, T. M., Liu, C., Chelton, D. B., Casey, K. S., and Schlax, M. G.: Daily high-

692 resolution-blended analyses for sea surface temperature, J Clim, 20, 5473–5496,

693 https://doi.org/10.1175/2007JCLI1824.1, 2007.

694 Rykaczewski, R. R., Dunne, J. P., Sydeman, W. J., García-Reyes, M., Black, B. A., and Bograd, S. J.:

695 Poleward displacement of coastal upwelling-favorable winds in the ocean's eastern boundary currents

696 through the 21st century, Geophys Res Lett, 42, 6424–6431, https://doi.org/10.1002/2015GL064694,

697 2015.

698 Sambe, B., Tandstad, M., Caramelo, A. M., and Brownd, B. E.: Variations in productivity of the Canary

699 Current Large Marine Ecosystem and their effects on small pelagic fish stocks, Environ Dev, 17, 105–

700 117, https://doi.org/10.1016/j.envdev.2015.11.012, 2016.

701 Santos, F., deCastro, M., Gómez-Gesteira, M., and Álvarez, I.: Differences in coastal and oceanic SST

702 warming rates along the Canary upwelling ecosystem from 1982 to 2010, Cont Shelf Res, 47, 1–6,

703 https://doi.org/10.1016/j.csr.2012.07.023, 2012.

704 Seabra, R., Varela, R., Santos, A. M., Gómez-Gesteira, M., Meneghesso, C., Wethey, D. S., and Lima,

705 F. P.: Reduced nearshore warming associated with eastern boundary upwelling systems, Front Mar Sci,

706 6, 445128, https://doi.org/10.3389/FMARS.2019.00104/BIBTEX, 2019.

707 Sherman, K. and Hempel, G.: The UNEP Large Marine Ecosystem Report: A perspective on changing

708 conditions in LMEs of the world's Regional Seas, UNEP Regional Seas Reports and Studies , 2008.

709 Siemer, J. P., Machín, F., González-Vega, A., Arrieta, J. M., Gutiérrez-Guerra, M. A., Pérez-

710 Hernández, M. D., Vélez-Belchí, P., Hernández-Guerra, A., and Fraile-Nuez, E.: Recent Trends in SST,

711 Chl-a, Productivity and Wind Stress in Upwelling and Open Ocean Areas in the Upper Eastern North

712 Atlantic Subtropical Gyre, J Geophys Res Oceans, 126, e2021JC017268,

713 https://doi.org/10.1029/2021JC017268, 2021.

714 Signorini, S. R., Franz, B. A., and McClain, C. R.: Chlorophyll variability in the oligotrophic gyres:

715 Mechanisms, seasonality and trends, Front Mar Sci, 2, 1–11, https://doi.org/10.3389/fmars.2015.00001,

716 2015.

717 Smale, D. A. and Wernberg, T.: Satellite-derived SST data as a proxy for water temperature in

718 nearshore benthic ecology, Mar Ecol Prog Ser, 387, 27–37, https://doi.org/10.3354/MEPS08132, 2009.

719 Sydeman, W. J., García-Reyes, M., Schoeman, D. S., Rykaczewski, R. R., Thompson, S. A., Black, B.

720 A., and Bograd, S. J.: Climate change and wind intensification in coastal upwelling ecosystems, Science

721 (1979), 345, 77–80, https://doi.org/10.1126/science.1251635, 2014.

722 Tel, E., Balbin, R., Cabanas, J. M., Garcia, M. J., Carmen Garcia-Martinez, M., Gonzalez-Pola, C.,

723 Lavin, A., Lopez-Jurado, J. L., Rodriguez, C., Ruiz-Villarreal, M., Sánchez-Leal, R. F., Vargas-Yáñez,

724 M., and Vélez-Belchí, P.: IEOOS: The Spanish Institute of Oceanography Observing System, Ocean

725 Science, 12, 345–353, https://doi.org/10.5194/OS-12-345-2016, 2016.

726 Wang, D., Gouhier, T. C., Menge, B. A., and Ganguly, A. R.: Intensification and spatial

727 homogenization of coastal upwelling under climate change, Nature, 518, 390–394,

728 https://doi.org/10.1038/nature14235, 2015.

729